INL/RPT-22-70445-Rev000

# Material and Design Optimization of Printed Melt Wire Arrays

November, 2022

*Summary Report — M4CT-22IN0702073*

Kiyo Fujimoto, Lance Hone, and Malwina Wilding
*Idaho National Laboratory*

*INL is a U.S. Department of Energy National Laboratory*
*operated by Battelle Energy Alliance, LLC*

INL/RPT-22-70445-Rev000

# Material and Design Optimization of Printed Melt Wire Arrays

## Summary Report — M4CT-22IN0702073

**Kiyo Fujimoto, Lance Hone, and Malwina Wilding**
**Idaho National Laboratory**

**November, 2022**

**Idaho National Laboratory**
**Idaho Falls, Idaho 83415**

**http://www.inl.gov**

**Prepared for the**
**U.S. Department of Energy**
**Office of Nuclear Energy**
**Under DOE Idaho Operations Office**
**Contract DE-AC07-05ID14517**

*Page intentionally left blank*

# SUMMARY

Recent work conducted by the Advanced Sensors and Instrumentation (ASI) program at Idaho National Laboratory resulted in the establishment of in-house capabilities for fabricating and testing new advanced manufactured sensors for measuring irradiation temperatures inside a nuclear test reactor. Though current methods of real-time temperature monitoring (e.g., thermocouples) can still be used, the complexity of the feedthroughs and attachments needed for collecting real-time measurements greatly increases the experiment-related costs. On the other hand, passive monitoring techniques can be used for collecting post-irradiation temperature measurements by inferring reactor temperatures, based on the melting points of well-characterized materials (i.e., standard melt wires). However, challenges have arisen due to the limited space available for including instrumentation in experiments. To resolve this issue, the ASI program expanded its temperature detection capabilities to include advance manufactured melt wires for post-irradiation temperature measurements. These melt wires can determine reactor temperatures while also accommodating space limitations in irradiation experiments. To improve performance reliability and enhance melt wire readability following irradiation, FY-22 efforts have focused on optimizing the materials used in the encapsulation and printed melt wire array. This report details the design and fabrication tasks, along with the subsequent x-ray computed tomography (XCT) evaluation process. The melt wire array consisted of indium with a melting point of 157°C, indium/silver (96/4 at%) with a melting point of 219°C, and tin with a melting point of 230°C. The encapsulation disc was made of vanadium due to its low activation properties and radiation resistance when deployed in nuclear reactors. Additionally, the melt wire design consisted of a ceramic sublayer (alumina disc) to further enhance the XCT post-melting images of the printed melt wires. However, when sealing the vanadium container, all three melt wires melted, reflecting the temperature limitations that must be considered when employing metal containers in the sealing process.

*Page intentionally left blank*

# ACKNOWLEDGEMENTS

This work was supported through the Nuclear Energy Enabling Technology (NEET) Advanced Sensors and Instrumentation (ASI) program, under Department of Energy (DOE) Idaho Operations Office contract no. DE-AC07-05ID14517. We thank James Milloway and Kurt Davis for their technical contributions to this work.

*Page intentionally left blank*

# CONTENTS



# FIGURES

# TABLES

# ACRONYMS

| | |
|---|---|
| AJP | aerosol jet printing |
| ASI | Advanced Sensors and Instrumentation |
| DEG | diethylene glycol |
| DSC | differential scanning calorimetry |
| PIE | post-irradiation examination |
| PVP | polyvinylpyrrolidone |
| TXRF | total x-ray fluorescence |
| XCT | x-ray computed tomography |

*Page intentionally left blank*

# Material and Design Optimization of Printed Melt Wire Arrays

## 1. INTRODUCTION

Irradiation testing affords insights into a wide range of radiation-induced phenomena, thereby fostering a better understanding of fuel/material performance in reactor environments. The recent focus on advanced reactor fuel types has further emphasized the need to better understand irradiation effects on fuel/material performance, thus necessitating investigation into new approaches to in-pile instrumentation development [1]. In this light, specialized experiments for material evaluations are key for ensuring the safety and reliability of advanced reactors. One key parameter in irradiation experiments is temperature, which is monitored via both passive and active techniques. Active monitoring techniques (e.g., thermocouples) provide real-time data but are usually expensive because of the engineering challenges associated with accommodating instrumentation leads. Passive monitoring techniques are typically used in static irradiation capsules to measure irradiation temperatures [2]. These passive techniques are preferred for temperature monitoring during irradiation tests in which less-expensive measurement methods are required, or in experiments that necessitate instrumentation without leads (e.g., static capsule experiments) [3].

As one such passive monitoring technique, melt wires enable researchers to identify the temperature ranges achieved during irradiation testing [4]. These melt wires are of a known composition and afford a well-characterized melting temperature under the given conditions or test environment. The irradiation temperature is inferred when, during post-irradiation examination (PIE), the wire is inspected for visual signs of melting. Such signs indicate that the irradiation temperature during testing exceeded the melting point of the wire material. On the other hand, if the wire does not show any signs of melting, this indicates that the irradiation temperature remained below the melting point of the wire material. These materials must be carefully selected before each melt wire package can be ready for use in irradiation experiments. The melt wire materials must also feature low neutron absorption cross sections, and all materials chosen for either the melt wires or the encapsulation could potentially react with each other or with a vapor alloy resulting from low eutectic points at high temperatures.

Based on a meticulous material selection process combined with rigorous validation procedures, the Measurement Science Laboratory at Idaho National Laboratory has produced a set of classical melt wire fabrication methods—including one that allows for encapsulating multiple wire materials into a single small-diameter quartz unit [5]. Over 40 qualified materials exist for use in melt wire fabrication, covering a temperature detection range of 29.73–1535°C [5]. While standard melt wires are commonly used in test reactor experiments—supported by materials test reactors such as the Advanced Test Reactor—sensor design is constrained by the predesigned capsules, whose geometries are imposed by the layout of the materials test reactor core. These capsules may only allow for sensors that are a couple of millimeters in diameter and feature prespecified geometries and placing multiple specimens simultaneously within the capsules may leave little to no space for instrumentation.

Production of robust miniature sensors is made possible through additive manufacturing techniques such as aerosol jet printing (AJP), inkjet printing, and micro-dispense printing. Incorporation of these technologies enables development of advanced sensors and instrumentation for reactors and fuel-cycle facilities, with printing patterns as small as 10 μm. These feature sizes aid in device miniaturization, especially considering that traditional melt wire capsules typically require a wire length of approximately 2 mm [6]. Through the advanced manufacturing portion of the Advanced Sensors and Instrumentation (ASI) program, novel technologies such as AJP are being explored for use in the development of unique sensors otherwise unobtainable via conventional fabrication processes. Past advanced manufactured melt wire development efforts and corresponding challenges are covered in [7], [8], and [9]. The development efforts conducted in FY-22 focused on further improving the melt wire encapsulation design and the material compatability between the melt wire arrays and encapsulation container. The goal was to

improve the readability of the x-ray computed tomography (XCT) results and minimize neutron activation of the printed melt wire package. Ultimately, the final material selected for the encapsulation container was vanadium. A printed ceramic sublayer (alumina disc) was introduced into the encapsulation, and the aerosol-jet-printed melt wires were created out of indium with a melting point of 157°C, indium/silver (96/4 at%) with a melting point of 219°C, and tin with a melting point of 230°C.

# 2. MATERIALS

Single- and multi-component metal nanoparticles were synthesized using the following materials: diethylene glycol (DEG) (Reagent Plus 99%, Sigma-Aldrich), N-methyl pyrrolidone (anhydrous, 99.5%, Sigma-Aldrich, α-terpineol [90%, Sigma-Aldrich]), sodium borohydride (99.99% [trace metal basis], Sigma-Aldrich), polyvinylpyrrolidone (PVP) (Sigma-Aldrich), tin acetate (99.99%, Sigma-Aldrich), silver nitrate (99.9999%, Sigma-Aldrich), and indium chloride (99.999% [trace metals basis], Sigma-Aldrich). Materials used for the x-ray fluorescence included Dow Corning high-vacuum grease and a quartz disc for each sample. Differential scanning calorimetry (DSC)/ thermogravimetric analysis (TGA) was conducted with alumina crucibles (DSC Consumables, 6.5 × 4 mm). For the purification process, centrifuge tubes were used for maintaining nanoparticles in suspension. The metallic pellet was resuspended in ethyl alcohol (>99.5%, Sigma-Aldrich) and acetone (Spectrum) throughout the purification process. The ceramic sublayer was fabricated using an alumina slurry (Admaprint, A130). The fabrication details are given in Section 4.1. All chemicals and reactants were used as received, without further modifications.

# 3. METHODS

This section of the report covers the encapsulation material selection, nanoparticle synthesis, and total x-ray fluorescence methods used for the designing of the printed melt wire package.

## 3.1 Vanadium Encapsulation

Previous iterations featured stainless steel 316 as the encapsulation material for the printed melt wires (see Figure 1). These printed samples were successfully hermetically sealed in inert gas and performed properly during furnace testing. However, the stainless steel caused challenges when reviewing the material via XCT. The XCT images of this material were somewhat unclear, as the visible contrast between the container and the printed wires was difficult to distinguish. For all printed melt wires, XCT is used for PIE, but without a method of obtaining a conclusive visual inspection, XCT can only minimally contribute to improving the traditional melt wire method. A redesign effort was completed to optimize all conceivably practical aspects of the encapsulation, with pure vanadium ultimately being selected as the applied material. Vanadium's melting point of 1910°C far exceeds those melting points of the melt wire materials used in previous experiments. This prevents all possibility of the container melting during the experiment and reduces the likelihood of any chemical interaction or vapor alloying occurring between the container and the melt wires. Vanadium's reasonably low thermal neutron absorption cross section (i.e., 5 barnes) prevents significant heat generation during irradiation, and is also beneficial in terms of its machining and welding capabilities. Although our machinist noted that, when machining vanadium, special care must be taken to avoid high temperatures during the sectioning and shaping of such small components, the container samples were fabricated with minimal error and loss of material (see Figure 2). Vanadium's weldability was also acceptable; and once the process was developed, the weld could be repeated without complications (see Section 4.3).

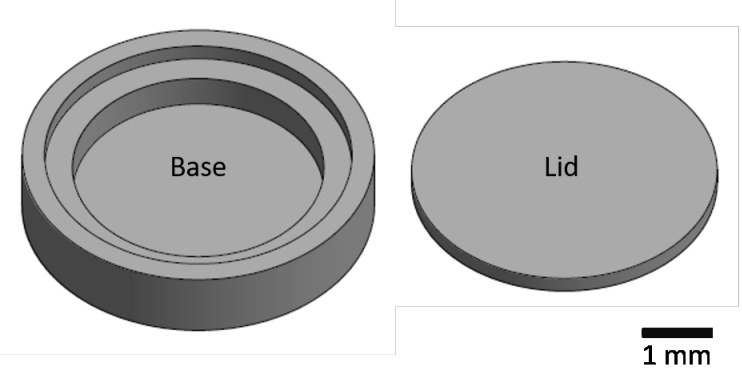


Figure 1. Design drawings of the melt wire encapsulation container.


Figure 2. Vanadium container for the printed melt wire package.

## 3.2 Nanoparticle Synthesis

Nanoparticle synthesis was accomplished via the method described in [4], but with some modifications. Table 1 gives an overview of the precursors used to create the functional nanoparticles of indium, indium/silver, and tin. To begin, 100 mL of DEG was degassed within a three-neck round-bottom flask. The degassing was done under reflux by bringing the solvent up to 200°C while purging under high argon flow for a minimum of 2 hours. The DEG was allowed to cool to room temperature before the PVP was added. Meanwhile, the metal salt precursors were dissolved in 10 mL of DEG. Next, sodium borohydride was dissolved in the vigorously stirred DEG and PVP solution. After 10 minutes, the metallic precursor solution was added dropwise (1 drop/sec) into the diethylene glycol, PVP, and sodium borohydride mixture. After the entirety of the metallic precursor solution was added, the suspension was continuously stirred overnight.

Table 1. Nanoparticle synthesis.

| Targeted Composition (at%) | Indium (III) Chloride (g) | Silver (III) Acetate (g) | Tin (III) Acetate (g) | 25 kDa Polyvinylpyrrolidone (g) | Sodium Borohydride (g) | Diethyleneglycol (mL) |
|---|---|---|---|---|---|---|
| Indium (100) | 0.561 | — | — | 1.04 | 1.01 | 100 |
| Tin (100) | 0.592 | — | — | 0.151 | 0.499 | 100 |
| Tin:Silver (96.5:3.5) | — | 0.014 | 0.518 | 0.151 | 0.502 | 100 |

Purification of nanoparticles to remove excess PVP capping agent and reaction byproducts was accomplished via centrifugation. The processing parameters were as follows. Each suspension of nanoparticles was transferred into a centrifuge test tube and placed in the centrifuge (Thermo Scientific, Legend XT). The samples were run at 9000 RPM for 5 minutes. After each run, the supernatant was discarded, and the pellet resuspended with ethanol. This was repeated at least five times per sample.

## 3.3 Total X-ray Fluorescence

Following purification, the samples were prepared for the total x-ray fluorescence (TXRF) equipment model Bruker S2 Picofox. A thin layer of silicon vacuum grease on the quartz discs created an adhesive surface upon which to deposit the dried powders. Each sample was run for a total of 1000 seconds per experiment, without any standard being used. In each result, silicon was identified as accounting for >50% of the composition. However, this was due to the vacuum grease. After accounting for all the detected elements, the target metal compositions were converted into atomic percentages, enabling comparison between the predicted and the experimental compositions. It is important to note that composition analysis was performed on the bi-metallic system, and not on individual particles. Individual particle composition is critical for determining a target peak temperature for each bi-metallic system. Any deviation can be attributed to experimental errors, variations in precursor concentrations, and the different reduction potentials associated with the two different elements.

# 4. FABRICATION

This section of the report will cover the fabrication of the ceramic sublayer, printing of melt wire array, and the encapsulation welding for the printed melt wire package.

## 4.1 Ceramic Sublayer

The ceramic encapsulation was designed in SOLIDWORKS, and the printed foils were created using digital light projection on an Admatech A130 with alumina slurry (Admaprint A130). The ceramic sublayer was then subjected to debinding and sintering to remove the organic binders and initial porosity to establish the defining microstructure and material properties. This process began by submerging the prints in water for 24 hours at 30°C to remove as much of the water-soluble components in the resin as possible. After soaking, the forms were wiped with a soft brush to remove any non-cured resin on the print surface. Next, the forms were dried in air for 24 hours. During the debinding step, organic components (binders) were removed with high temperature, and for the alumina, the following debinding heating profile was used: (1) starting at room temperature, ramp the furnace to 150°C at a rate of 60°C/hour, (2) remain at 150°C for 30 minutes, (3) ramp the furnace to 450°C at a rate of 12°C/hour, (4) ramp the furnace to 1000°C at a rate of 60°C/hour, (5) remain at 1000°C for 120 minutes, and (6) bring the furnace back down to room temperature at a rate of 100°C/hour. Once the debinding step was completed, the pieces were sintered to allow the alumina particles within the print to come in close contact with each another. This increases the density of the print and thus shrinks the overall dimensions. The sintering step was completed using the following heating profile: (1) starting at room temperature,

ramp the furnace to 1000°C at a rate of 200°C/hour, (2) remain at 100°C for 30 minutes, (3) ramp the furnace to 1575°C at a rate of 100°C/hour, (4) perform a second ramp to 1625°C at 75°C/hour, (5) remain at 1625°C for 120 min, and (6) bring the furnace down to room temperature at a rate of 300°C/hour. The final product is seen in Figure 3.

Figure 3. Ceramic sublayer discs for the printed melt wire package. Left: Top cap. Right: Slots for printing the melt wires.

## 4.2 Melt Wire Printing

Fabrication of the advanced manufactured melt wires was achieved via AJP (IDS Nanojet). The formulated ink used in all the experiments was 60 vol% N-methyl pyrrolidone, 20 vol% α-terpineol, and 20 vol% nanoparticle suspension. The precursor nanoparticle suspension consisted of 60 w/v% PVP-capped indium, tin/silver, or tin nanoparticles in N-methylpyrrolidone. During printing, the tool platen temperature (45°C), aerosol gas, sheath gas, and print speed were optimized to ensure that the line widths and material deposition of functional materials were adequate to obtain the desired device dimensions. Prior to printing, the printed alumina sublayer was rinsed with acetone and ethanol in an ultrasonic bath to clean the substrate surface. The printed melt wires (Figure 4) were fabricated to be 1.5 mm (L) × 0.25 mm (W). After printing, the melt wires were sintered in an argon glovebox at 100°C for 1 hour to minimize oxidation while sintering, as well as to remove any residual solvent.

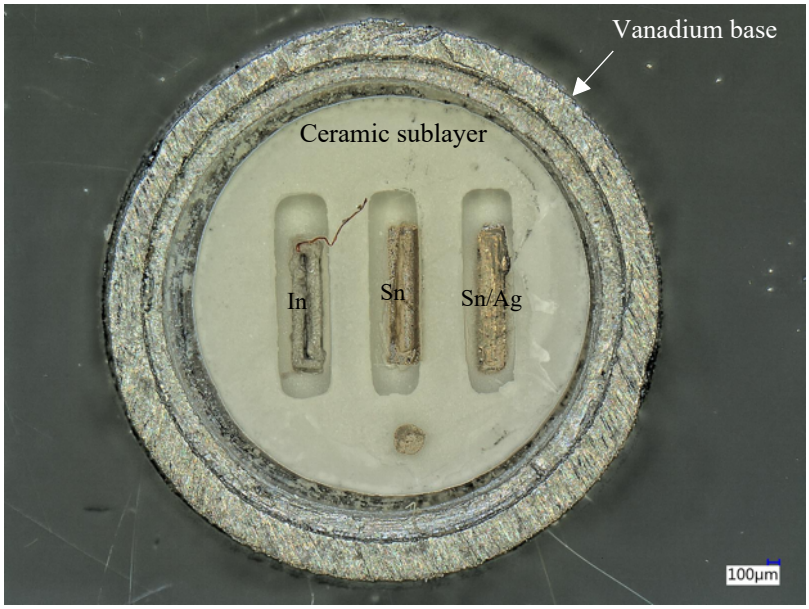


Figure 4. Printed melt wires on the ceramic sublayer that's placed inside the vanadium base.

## 4.3 Encapsulation Welding

The welding was accomplished using a precision laser welder at 110 W. Although there was minimal uncertainty in welding the vanadium, one major concern regarding the encapsulation was premature exposure of the melt wires to high temperatures during the laser welding process. To avoid this, certain geometric changes were made to the previous container design. First, the container height was increased from 1 to 2 mm, allowing more surface area to be cradled by the copper heat sink material to draw heat away as the energy was applied during the laser weld. Second, the inner ceramic sublayer was designed to reduce conductive heat transfer during welding. This sublayer serves as the substrate for up to three melt wires within a single encapsulation. Each melt wire is printed into a separate slot in the inner capsule (Figure 5). The entire ceramic insert design has a height of .75 mm and an outer diameter of 3.5 mm. Each slot has a length of 2 mm, a width of 0.5 mm, and a depth of 0.25 mm. A wafer-thin ceramic covering reduces the conductivity between the wires and the vanadium encapsulation lid. The ceramic sublayer was also designed for the secondary purpose of providing more detailed XCT images (see Section 5.3). Thanks to material property differences between a ceramic and the printed melt wires and encapsulation materials, the wire(s) appear suspended within the enclosure, thus enabling them to be clearly distinguished from the surrounding container.

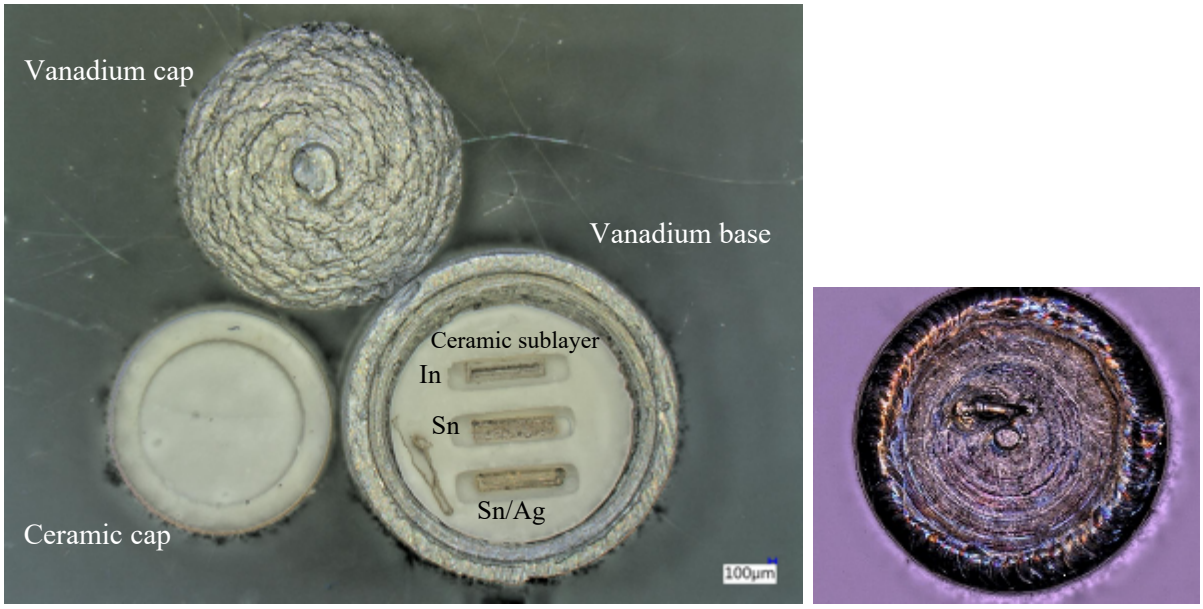


(a) (b)

Figure 5. (a) The entire printed melt wire package prior to welding the vanadium container. (b) Post-welding.

# 5. EVALUATION

This section of the report will cover evaluation of the printed melt wire package using Total X-ray Fluorescence (TXRF), differential scanning calorimetry (DSC), and X-ray Computed Tomography (XCT) equipment.

## 5.1 Evaluation of Total X-ray Fluorescence

The TXRF analysis was performed using a Bruker S2 Picofox, and the respective bi-metallic compositions are shown in Table 2. It is important to note that, for the multi-component systems, composition analysis was performed on the bi-metallic system and not on the individual particles. Individual particle composition is critical for determining a target peak temperature for each bi-metallic system. For this work, two single-element and one bi-metallic material were chosen to provide a melting point temperature range of 157–232°C. For the single-element nanoparticles, the TXRF results were as expected. The bi-metallic system (tin/silver) nanoparticle compositions were selected from the binary phase diagram and identifying the eutectic composition, as the nanoparticle compositions tend toward those compositions. During the synthesis process, metal salt precursor amounts were determined by establishing a targeted mass for each nanoparticle system and then adjusting the precursor amounts to create the desired nanoparticle composition.

Table 2. Melting point of the synthesized nanoparticles.

| Nanoparticle System | Theoretical Composition (at%) | Experimental Composition (at%) |
|---|---|---|
| Tin | 100 | 1:0 |
| Tin:Silver | 96.5:3.50 | 98.4:1.60 |
| Indium:Silver (1:0) | 100:0 | 1:0 |

## 5.2 Differential Scanning Calorimetry

DSC detects endothermic and exothermic transitions, and even determines the transformation temperatures and the enthalpy of solids and liquids as a function of temperature. For the present analysis, 5 to 50 mg of sample material was loaded into an alumina crucible (DSC Consumables, DSC72001) that was then closed and placed in the DSC/ thermogravimetric analysis (TGA) (STA 449 F3, Netzsch) to run. The theoretical and actual melting points were estimated from phase diagrams (see Figure 6 and Figure 7) and derived from DSC, respectively, and are presented in **Table 3.**

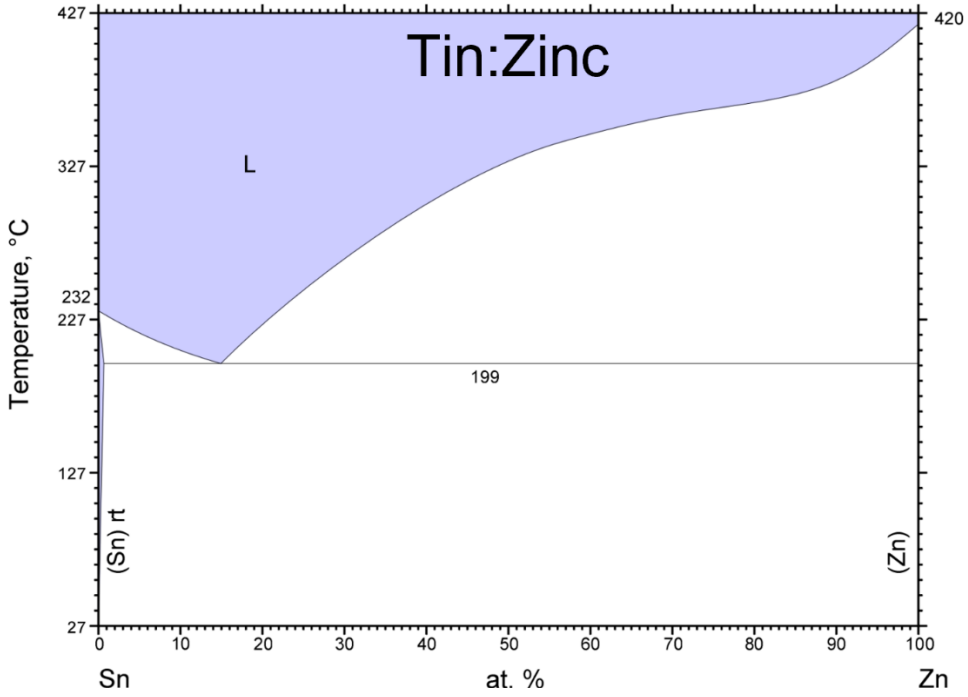


Figure 6. Tin/zinc phase diagram [5].

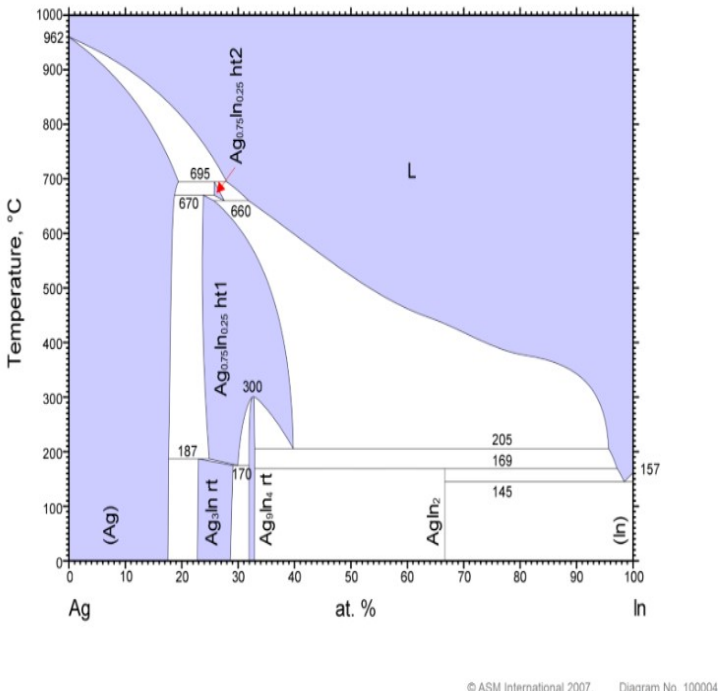


Figure 7. Silver/indium phase diagram [8].

Table 3. Melting points of the synthesized nanoparticles.

| Nanoparticle System | Theoretical Composition (at.%) | Targeted Melting Point (°C) | Theoretical Melting Point* (°C) | DSC Melting Point (°C) |
|---|---|---|---|---|
| Tin: Silver | 1:0 | 231 | 231 | 230.3 |
| Tin:Silver | 96.5:3.50 | 221 | 230 | 219.4 |
| Indium:Silver (1:0) | 1:0 | 157 | 157 | 157.3 |

For this work, the current list of melt wire materials was used as a guide when selecting the individual components. Next, a review of certain binary phase diagrams was performed to determine which systems would provide a melting point range of less than 100°C when fabricating an array consisting of three different advanced manufactured melt wires. Based on this review, tin/silver (96.5/3.5%) was selected as the material that best meet those requirements (see Figure 7). According to previous experiments, if a relatively deep eutectic is observed, the concentration of the nanoparticles will favor that point. Thus, the eutectic composition for tin/silver was identified. The experiment and theoretical melting points for tin, tin/silver (96.5/3.5%), and indium were all in agreement.

## 5.3 X-ray Computed Tomography

XCT was used to produce detailed images of the melt wires both before and after welding the vanadium container. Since different materials have different melting characteristics, it is important to identify features that result from melting, such as the formation of newly rounded edges or formation of the whole melted line into a sphere, or of bubbles/beads despite the bulk of the material appearing unaffected. XCT images from previous work [9] provided accurate measurements at resolutions as high as 50 µm, and a software was employed that could measure features as small as 4 µm. This drastically improved the ability to identify the potential unique melting characteristics of each material. It is important to note that the melt wire evaluation method discussed in this report is the same as what would

be used to evaluate these containers during PIE. Evaluation of melt wires is accomplished by obtaining, prior to the experiment, an initial XCT image of a sealed melt wire assembly to serve as a reference point. After the experiment, a new XCT image will be obtained for comparison against the reference image to determine whether any changes have occurred. Part of the fabrication process involves applying the same imaging techniques used for PIE to the testing of prototypes made from each material to identify any characteristics that indicate whether melting has occurred.

Since the melt wire array featured much lower melting points (157–230°C) than what had been used previously, the melt wires were able to be pre-melted during the vanadium sealing process. Unlike traditional melt wires, which have quartz tubing to isolate and seal each of them under an inert atmosphere, the printed melt wires rely on a metal encapsulation that affords poorer heat transfer control. Even adding the ceramic sublayer failed to help with the pre-melting, such that all three melt wires melted during the encapsulation process. Figure 8 clearly shows the middle melt wire (Sn) to be almost gone, with only the slight residue on the right-hand side indicating that melting had occurred. Since tin had the highest melting point (i.e., 230°C), it can be inferred that the other two melt wires melted as well. This is shown in Figure 9, with the deformation of both the outer melt wires (In and Sn/Ag) indicating that melting has occurred. To improve the sealing process, printed melt wires should be sealed in a glovebox under an inert atmosphere. Altering the welding process to minimize heat generation is also needed.

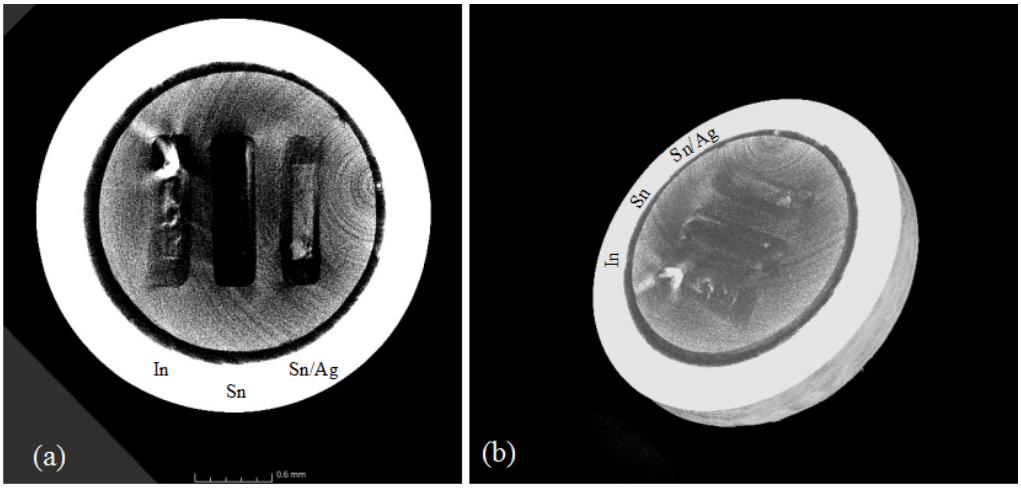

Figure 8. XCT images of the melt wires: (a) top view and (b) 3D view.

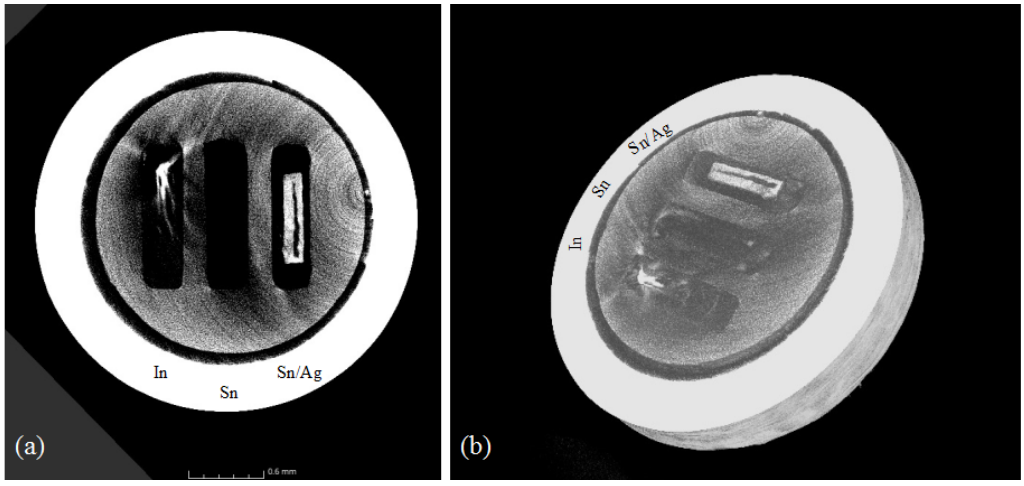

Figure 9. XCT images of the melt wires at different angles: (a) top view and (b) 3D view.

# 6. CONCLUSION

Recent work conducted by the ASI program at Idaho National Laboratory resulted in the establishment of in-house capabilities for fabricating and testing new advanced manufactured sensors for measuring irradiation temperatures inside a nuclear test reactor. Though current methods of real-time temperature monitoring (e.g., thermocouples) can still be used, the complexity of the feedthroughs and attachments needed for collecting real-time measurements greatly increases the experiment-related costs. On the other hand, passive monitoring techniques can be used for collecting post-irradiation temperature measurements by inferring reactor temperatures, based on the melting points of well-characterized materials (i.e., standard melt wires). However, challenges have arisen due to the limited space available for including instrumentation in experiments. To resolve this issue, the ASI program expanded its temperature detection capabilities to include advanced manufactured melt wires for post-irradiation temperature measurements. These melt wires can determine reactor temperatures while also accommodating space limitations in irradiation experiments. To improve performance reliability and enhance melt wire readability following irradiation, FY-22 efforts have focused on optimizing the materials used in the encapsulation and printed melt wire array. This report details the design and fabrication tasks, along with the subsequent XCT evaluation process. The melt wire array consisted of indium with a melting point of 157°C, indium/silver (96/4 at%) with a melting point of 219°C, and tin with a melting point of 230°C. The encapsulation container was made of vanadium due to its low activation properties and radiation resistance when deployed in nuclear reactors. Additionally, the melt wire design consisted of a ceramic sublayer (alumina disc) to further enhance the XCT post-melting images of the printed melt wires. However, when sealing the vanadium container, all three melt wires melted, reflecting the temperature limitations that must be considered when employing metal containers in the sealing process.

# 7. REFERENCES


1. Calderoni, P., D. Hurley, J. Daw, A. Fleming, and K. McCary, "Innovative sensing technologies for nuclear instrumentation," *2019 IEEE International Instrumentation and Measurement Technology Conference (12MTC)*, 2019, pp. 1-6. https://doi.org/10.1109/I2MTC.2019.8827129.
2. Bong Goo, K., J. L. Rempe, J. F. Villard, and S. Solstad, "Review of Instrumentation for Irradiation Testing of Nuclear Fuels and Materials," Nuclear Technology, **176**, 2, 155–187 (2011). [Taylor & Francis Online]. https://doi.org/10.13182/NT11-A13294.
3. Marshall, Frances M. 2005. "Advanced Test Reactor Capabilities and Future Operating Plans." INL/CON-05-00549, Idaho National Laboratory. https://www.osti.gov/biblio/911161.
4. Daw, J. E. et al., "Temperature Monitoring Options Available at the Idaho National Laboratory Advanced Test Reactor," AIP Conference Proceedings **1552**, 1, 970–975 (2013). https://doi.org/10.1063/1.4819675.
5. Davis, K. L., D. L. Knudson, J. E. Daw, J. L. Rempe, and A. J. Palmer, 2012. "Melt Wire Sensors Available to Determine Peak Temperatures in ATR Irradiation Testing," *Eighth American Nuclear Society International Topical Meeting on Nuclear Plant Instrumentation, Control and Human-Machine Interface Technologies. Enabling the Future of Nuclear Energy*. INL/CON-11-23913, Idaho National Laboratory. https://www.osti.gov/biblio/1054299.
6. Seifert, T., E. Sowade, F. Roscher, M. Wiemer, T. Gessner, and R. R. Baumann, "Additive Manufacturing Technologies Compared: Morphology of Deposits of Silver Ink Using Inkjet and Aerosol Jet Printing," Industrial and Engineering Chemical Research, **2015,** 54 (2), 769–779. https://doi.org/10.1021/ie503636c.
7. Mondal, K., K. Fujimoto, and M. D. McMurtrey, "Advanced Manufacturing of Printed Melt Wire Chips for Cheap, Compact Passive In-Pile Temperature Sensors," *Jom*, **72**, 12, 4196–4201 (2020). https://doi.org/10.1007/s11837-020-04426-8.

8. Mondal, K., K. Fujimoto, and M. McMurtrey. 2020. “Non-visual Analysis of Miniaturized Melt Wire Arrays for In-pile Measurement of Peak Irradiation Temperature,” INL/EXT-20-57468, Idaho National Laboratory. https://doi.org/10.2172/1668675.
9. Hone, L., K. Fujimoto, K. Manning, and M. Wilding, 2021. “Design Optimization for Printed Melt Wire Arrays Encapsulation,” INL/EXT-21-63886, Idaho National Laboratory. https://www.osti.gov/biblio/1826589.